

# The Mount Hickman ultramafic complex: An Fe-rich Alaskan-type ultramafic intrusion



Dejan Milidragovic<sup>1,2,a</sup>, Alex Zagorevski<sup>3</sup>, and John B. Chapman<sup>2</sup>

<sup>1</sup>present address, British Columbia Geological Survey, Ministry of Energy and Mines, Victoria, BC, V8W 9N3

<sup>2</sup>Geological Survey of Canada, 1500-605 Robson Street, Vancouver, BC, V6B 5J3

<sup>3</sup>Geological Survey of Canada, 601 Booth Street, Ottawa, ON, K1A 0E8

<sup>a</sup>corresponding author: Dejan.Milidragovic@gov.bc.ca

Recommended citation: Milidragovic, D., Zagorevski, A., and Chapman, J.B., 2017. The Mount Hickman ultramafic complex: An Fe-rich Alaskan-type ultramafic intrusion. In: Geological Fieldwork 2016, British Columbia Ministry of Energy and Mines, British Columbia Geological Survey Paper 2017-1, pp. 117-132.

**Abstract**

The Mount Hickman ultramafic complex (Triassic) is a composite Alaskan-type ultramafic pluton in Stikine terrane, northwestern British Columbia. Cumulate rocks in the complex are mainly olivine ±magnetite clinopyroxenite, but include subordinate serpentized dunite, wehrlite, and gabbro. Magnetite is a volumetrically significant primary phase, especially in magnetite-olivine clinopyroxenite, where it may constitute up to 40% by volume. In contrast to most other Alaskan-type intrusions, and terrestrial ultramafic plutons in general, the Mount Hickman ultramafic complex has an unusually high concentration of FeO<sup>TOT</sup>, including ~21 wt.% in dunite. We currently favour a model in which the high contents of FeO<sup>TOT</sup> in the Mount Hickman ultramafic complex reflect mixing of two types of magma: a relatively primitive ultramafic (picritic/basaltic silicate magma, and a dense Fe-Ti-P-rich highly oxidized magma.

**Keywords:** Hickman ultramafic complex, Alaskan-type intrusion, Triassic, Stikinia, cumulate

**1. Introduction**

The Stikine terrane (Paleozoic to Mesozoic) of the Canadian Cordillera (Fig. 1) experienced a period of arc building and extensive mineralization during the Middle to Late Triassic. This period was marked by ultramafic to intermediate volcanism and related sedimentation (Stuhini and Lewes River groups; Mihalynuk et al., 1999; Logan et al., 2000) and intermediate to felsic plutonism of both calc-alkaline (~228-215 Ma Stikine suite) and alkaline (~215-200 Ma; Copper Mountain suite) affinities (Woodsworth et al., 1991; Zagorevski et al., 2016). Alaskan-type mafic-ultramafic intrusions, defined by the association of olivine, clinopyroxene, and hornblende, and complete lack of orthopyroxene (Taylor, 1967; Nixon et al., 2015) represent a volumetrically minor component of this period. Nonetheless, their petrogenetic significance and relationship to coeval igneous rocks of Stikine terrane are poorly understood.

Woodsworth et al. (1991) introduced the term ‘Polaris suite’ for Late Triassic Alaskan-type intrusions in the northern Cordillera. However, more recent work has demonstrated that these intrusions formed from the Middle Triassic to the Early Jurassic (237 ±2 Ma, Lunar Creek complex, Nixon et al., 1997; 186 ±2 Ma, Polaris complex, Nixon et al., 1997; 190 ±1 Ma Turnagain intrusion, Scheel, 2007) in both Stikine and Quesnel terranes. Because of potential confusion about use of ‘Polaris suite’, we avoid the term in this paper.

The Mount Hickman ultramafic complex is an Alaskan-type intrusion exposed on the southeastern margin of the Hickman pluton (Fig. 2; ~220-222 Ma; Holbek 1988; Nixon et al., 1989;

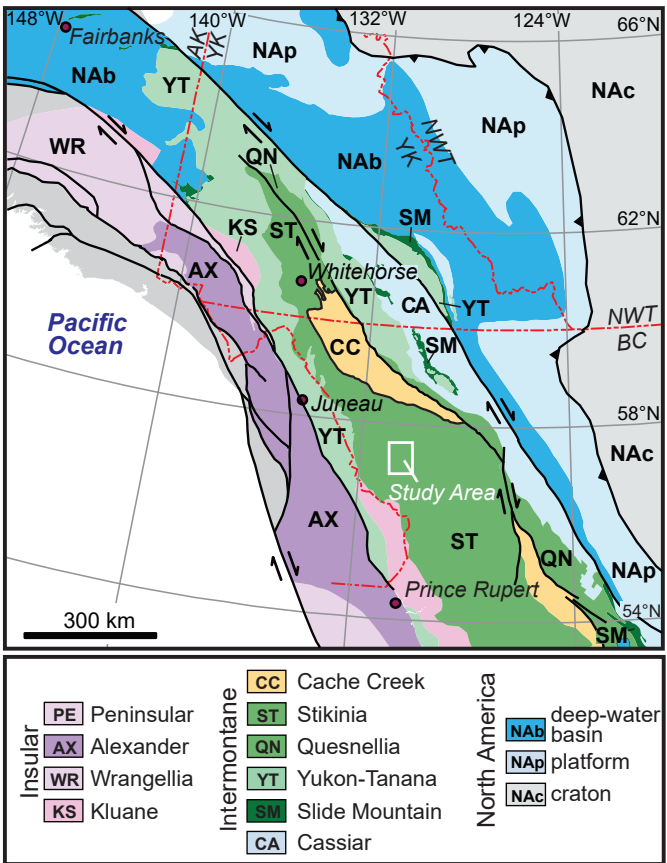


Fig. 1. Terrane map of the northern Canadian Cordillera showing the location of the study area (modified from Nelson et al., 2013).

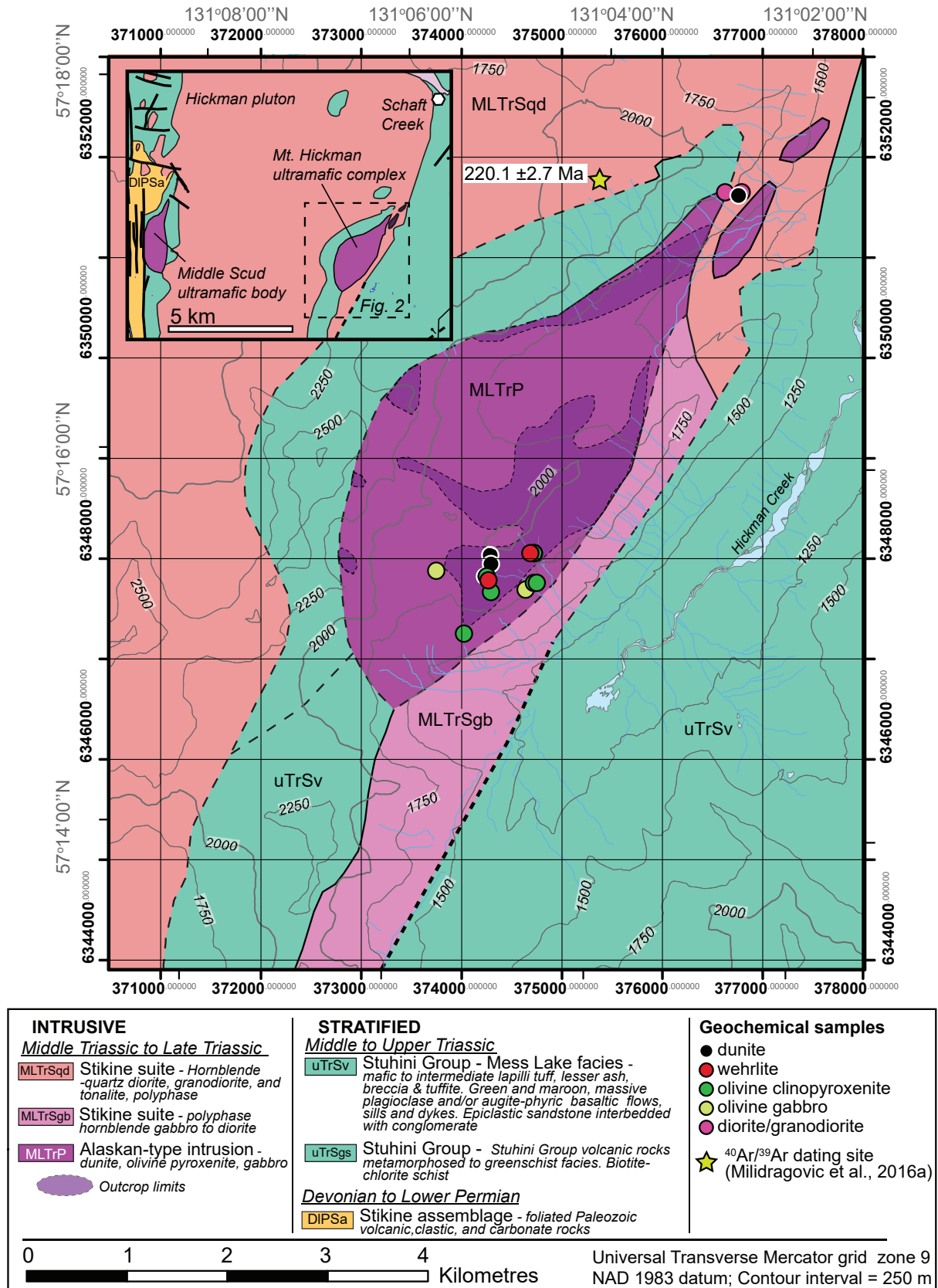


Fig. 2. Geological map of the Mount Hickman ultramafic complex (modified after Brown et al., 1996, Mihalynuk et al., 1996, and Milidragovic et al., 2016a), showing the locations of samples analyzed for geochemistry (Table 1). Inset: regional geology map, showing the location of the Mount Hickman ultramafic complex, the Middle Scud ultramafic body, and the Schaft Creek exploration camp.

Milidragovic et al., 2016a). This report provides a petrographic and geochemical description of the principal rock types in the Mount Hickman ultramafic complex, and a comparison to the nearby Middle Scud ultramafic body on the west side of the Hickman pluton (Fig. 2 inset).

## 2. Geological setting

The Stikine terrane is a composite Devonian to Jurassic volcanic arc consisting mainly of volcanosedimentary and plutonic rocks. The first of three episodes of island-arc formation is recorded by the Stikine assemblage (Paleozoic; Monger, 1977). The second is recorded by the Stuhini Group (Middle-Upper Triassic), which unconformably overlies the Stikine assemblage and consists of predominantly subaqueous mafic to felsic volcanic and related sedimentary rocks. Unconformably above the Stuhini Group, the Hazelton Group (Lower-Middle Jurassic) represents the third episode, and contains subaqueous to subaerial, volcano-sedimentary rocks (e.g., Brown et al., 1996; Logan et al., 2000; Barresi et al., 2015). Plutonic suites coeval with these episodes include: Forrest Kerr (Late Devonian); More Creek (Early Mississippian); Stikine, Alaskan-type and Copper Mountain (Late Triassic); Texas Creek, Aishihik, and Long Lake (Early Jurassic); and Three Sisters (Middle Jurassic; Logan et al., 2000; Zagorevski et al., 2016). The Hickman pluton, north and west of the Mount Hickman ultramafic complex (Fig. 2), is a composite intrusion and part of the Stikine suite (Brown et al., 1996; Logan et al., 2000).

The Mount Hickman ultramafic complex is an elongate, northeast-trending, ultramafic intrusion, approximately 6 km long and 3 km wide (Fig. 2; Holbek, 1988; Brown and Gunning, 1989; Nixon et al., 1989). Previous work described the Mount Hickman ultramafic complex as a zoned intrusion containing minor serpentized dunite, (olivine) clinopyroxenite, and gabbro (Holbek, 1988; Nixon et al., 1989). The range of observed rock types qualifies the Mount Hickman ultramafic complex as an Alaskan-type intrusion, (see Taylor, 1967; Nixon et al., 2015). Along its western margin, the Mount Hickman ultramafic complex is in contact with plagioclase-phyric andesite of probable Stuhini Group affinity (Brown and Gunning, 1989; Nixon et al., 1998; Brown et al., 1996). Brown and Gunning (1989) and Nixon et al. (1989) interpreted this contact as intrusive, implying that complex is Middle Triassic or younger. The northern margin of the Mount Hickman ultramafic complex is truncated by the main phase of the Hickman pluton (Brown and Gunning, 1989; Nixon et al., 1989). Rubidium-Strontium, K-Ar and  $^{40}\text{Ar}/^{39}\text{Ar}$  ages of ~220-222 Ma on biotite and hornblende from the Hickman pluton (Holbek, 1988; Milidragovic et al., 2016a) indicate that the Mount Hickman ultramafic complex is Late Triassic or older.

The Middle Scud ultramafic body is ~15 km west of the Mount Hickman ultramafic complex, separated from it by the Mount Hickman pluton (Fig. 2 inset). The Middle Scud body intrudes mafic metavolcanic rocks of probable Stuhini Group affinity and is intruded by the main phase of the Hickman

Pluton (Brown et al., 1996). The Middle to Late Triassic age, the predominantly olivine and clinopyroxene mineralogy, and proximity to the Mount Hickman complex suggest that the Middle Scud ultramafic body may be genetically related to the Mount Hickman complex.

## 3. Analytical methods

Nineteen samples collected in 2015 were analyzed at Activation Laboratories (Ancaster, ON) for whole-rock major and trace element compositions (Table 1), using the 4Lithores analytical package. Samples, pulverized using an agate mill, were mixed with a flux of lithium metaborate/tetraborate, fused, and dissolved in nitric acid. The concentrations of major and selected trace elements (Sc, V, Be, Ba, Sr, and Zr) were measured by inductively coupled plasma-optical emission spectrometry (ICP-OES). The remaining trace elements, including REE, were determined by inductively coupled plasma-mass spectrometry (ICP-MS). The relative uncertainty in measurement, at a 95% confidence interval, is  $\leq 6\%$  for most major elements. Due to low concentrations, the relative uncertainty in the measurement of  $\text{Na}_2\text{O}$ ,  $\text{K}_2\text{O}$ , and  $\text{P}_2\text{O}_5$  is larger; near the quantification limit (defined as 3.33 times the detection limit), the relative uncertainty is ~30% for  $\text{Na}_2\text{O}$  and  $\text{P}_2\text{O}_5$  and ~50% for  $\text{K}_2\text{O}$ . The uncertainty in most trace element concentrations varies between  $< 5\%$  relative (Cr, Ni) to  $\leq 40\%$  relative (Nb, Ta, Hf) at the 95% confidence level. The relative uncertainty in concentration of rare earth elements (REE), Y, Zr, Th, and U is  $\leq 25\%$ , whereas the relative uncertainty in the measurement of large ion lithophile elements (LILE) varies from ~5% (Sr) to  $\leq 40\%$  (Ba).

The composition of olivine (Table 2) was measured at the University of British Columbia (Vancouver, BC) on a Cameca SX50 electron microprobe. Analyses by wavelength dispersive spectrometry (WDS) were performed using 20 kV accelerating voltage, 15 nA beam current, and 5 mm beam diameter. Errors in  $\text{SiO}_2$  and MgO measurements on olivine are  $< 1\%$  relative ( $2\sigma$ ), whereas the uncertainty in FeO measurement is  $\leq 3\%$  relative. The relative uncertainty in minor oxide constituents of olivine (NiO, MnO) is typically  $< 50\%$ . The concentrations of  $\text{TiO}_2$ ,  $\text{Al}_2\text{O}_3$ ,  $\text{Cr}_2\text{O}_3$ , and CaO in olivine are near or below detection limit.

## 4. Main rock types of the Mount Hickman ultramafic complex

Glaciers and scree obscure large parts of the Mount Hickman ultramafic complex, which consists of serpentized dunite, wehrlite, olivine clinopyroxenite, and olivine gabbro. Olivine clinopyroxenite is volumetrically the most abundant rock type; pods and slivers of dunite (Fig. 3) and wehrlite are volumetrically minor and exposed in the southeastern and northeastern parts of the intrusion. Olivine gabbro is limited to isolated outcrops in the southern part of the intrusion. Concentric zoning from a dunite core, through peridotite and clinopyroxenite ( $\pm$ hornblende  $\pm$ magnetite), to a feldspathic rim, which is sometimes considered as a defining characteristic



Table 1. Continued.

Sample #	ZE15SB 54 <sup>a</sup>	ZE15SB 55A <sup>a</sup>	ZE15DM4 08C <sup>a</sup>	ZE15DM4 09A <sup>a</sup>	ZE15DM4 08A <sup>a</sup>	ZE15DM7- 03D <sup>b</sup>	ZE15DM7- 03F <sup>b</sup>	ZE15DM7- 03E <sup>b</sup>	ZE15-DM7- 03C <sup>b</sup>
Easting	374611	373751	376720	376611	376720	361699	361699	361699	361699
Northing	6347728	6347894	6351625	6351660	6351625	6349640	6349640	6349640	6349640
Lithology	ol. gabbro	gabbro	hbl. diorite	hbl. diorite	Granodiorite dyke	wehrlite	wehrlite	ol. hbl'd'te	bt. wehrlite
Major elements (wt.%)									
SiO <sub>2</sub>	46.08	46.08	57.96	55.93	67.84	39.55	41.49	44.15	42.56
TiO <sub>2</sub>	0.20	0.20	0.56	0.64	0.24	0.58	0.24	0.35	0.62
Al <sub>2</sub> O <sub>3</sub>	20.68	20.68	18.22	18.37	15.46	5.68	2.77	6.18	7.12
Fe <sub>2</sub> O <sub>3</sub>	4.65	4.65	5.63	8.05	2.68	11.27	10.63	10.31	10.78
MnO	0.19	0.10	0.14	0.16	0.04	0.16	0.15	0.15	0.14
MgO	8.58	8.58	2.44	3.19	1.00	26.90	31.64	25.37	22.76
CaO	12.70	16.78	5.10	4.99	1.96	6.49	6.07	7.34	9.09
K <sub>2</sub> O	1.18	3.02	2.95	2.07	3.61	0.70	0.02	0.47	2.25
Na <sub>2</sub> O	2.00	0.21	4.81	4.65	4.97	0.49	0.27	0.92	0.57
P <sub>2</sub> O <sub>5</sub>	0.07	<0.01	0.30	0.22	0.10	0.03	0.03	0.10	0.02
LOI	1.55	3.26	1.78	2.53	1.58	7.55	4.75	2.83	4.23
Total	100.10	100.80	99.88	100.50	99.47	99.40	98.07	98.19	100.10
<sup>c</sup> Mg#	0.57	0.71	0.46	0.44	0.43	0.83	0.85	0.83	0.81
Trace elements (ppm)									
Cs	0.5	1.1	0.5	1.1	0.4	0.1	<0.1	0.3	0.5
Rb	19	72	53	46	58	10	<1	8	40
Ba	329	902	799	552	1178	42	10	322	348
Th	0.15	<0.05	2.20	1.08	2.80	<0.05	<0.05	0.21	<0.05
U	0.09	0.03	1.43	0.62	3.87	0.01	<0.01	0.2	0.01
Nb	0.7	<0.2	4.8	1.7	6.0	0.4	<0.2	0.3	0.3
Ta	0.07	0.04	0.30	0.15	0.34	0.06	0.04	0.05	0.07
Pb	<5	<5	<5	<5	<5	<5	<5	<5	<5
Sr	771	515	689	598	395	38	71	168	58
Zr	14	7	81	69	91	14	6	17	14
Hf	0.6	0.2	1.8	1.7	1.9	0.4	0.2	0.5	0.5
Y	9.6	4.4	13.5	17.4	5.9	7.7	4.1	6.9	8.5
Ga	13	10	18	16	16	6	3	6	7
Sc	45	46	10	12	2	31	18	23	30
V	346	117	171	147	48	158	106	151	181
Co	44	20	10	14	5	80	85	75	72
Zn	70	<30	40	60	30	60	60	60	50
Cu	40	170	30	20	10	10	<10	70	<10
Cr	170	170	30	20	30	1350	1920	1770	1200
Ni	70	40	<20	20	<20	960	1320	950	810
La	2.57	1.58	13.10	9.11	9.36	0.61	0.59	2.10	0.95
Ce	5.76	2.52	24.20	19.10	15.90	2.51	1.33	4.27	2.76
Pr	0.86	0.31	2.95	2.38	1.73	0.50	0.25	0.64	0.57
Nd	5.04	1.70	12.70	11.40	6.68	2.82	1.41	3.28	3.03
Sm	1.69	0.68	2.83	2.68	1.18	1.38	0.50	1.04	1.22
Eu	0.582	0.319	0.946	0.995	0.469	0.372	0.197	0.333	0.421
Gd	1.84	0.82	2.70	3.24	1.08	1.42	0.67	1.20	1.49
Tb	0.33	0.14	0.43	0.49	0.14	0.24	0.12	0.19	0.25
Dy	1.98	0.83	2.39	2.88	0.91	1.39	0.82	1.14	1.50
Ho	0.36	0.15	0.48	0.58	0.19	0.28	0.16	0.24	0.29
Er	0.95	0.39	1.34	1.72	0.59	0.76	0.40	0.68	0.82
Tm	0.139	0.054	0.195	0.264	0.094	0.104	0.058	0.098	0.117
Yb	0.85	0.33	1.41	1.80	0.71	0.63	0.36	0.60	0.74
Lu	0.119	0.048	0.210	0.265	0.131	0.095	0.057	0.086	0.107

<sup>a</sup> Mount Hickman ultramafic complex. <sup>b</sup> Middle Scud ultramafic body. <sup>c</sup> Minimum Mg-number defined as Mg/(Mg+Fe<sup>2+</sup>), where all Fe is expressed as Fe<sup>2+</sup>.

**Table 2.** Average olivine compositions from the Mount Hickman ultramafic complex and the Middle Scud ultramafic body.

Sample:	ZE15-DM4-01B	ZE15-DM4-01A	ZE15-SB53	ZE15-DM7-03F
<sup>1</sup> n	3	8	9	14
Area	Hickman	Hickman	Hickman	
Rock	ol. cpxite	wehrlite	mt. ol. cpxite	wehrlite
<sup>2</sup> WR Mg#	0.79	0.79	0.57	0.85
SiO <sub>2</sub>	39.2 ±0.3	39.2 ±0.4	38.9 ±0.6	41.0 ±0.5
TiO <sub>2</sub>	<0.06	<0.06	<0.06	<0.06
Al <sub>2</sub> O <sub>3</sub>	<0.04	<0.04	<0.04	<0.04
MgO	39.8 ±0.4	40.3 ±0.4	38.8 ±0.6	47.8 ±0.4
FeO	20.1 ±0.1	19.7 ±0.5	21.6 ±0.7	10.7 ±0.3
MnO	0.41 ±0.06	0.45 ±0.04	0.55 ±0.06	0.20 ±0.05
CaO	0.06 ±0.02	0.06 ±0.04	<0.06	<0.06
NiO	<0.15	<0.15	<0.15	<0.15
Cr <sub>2</sub> O <sub>3</sub>	<0.12	<0.12	<0.12	0.30 ±0.07
Total	99.7 ±0.7	99.9 ±0.7	99.9 ±0.8	100.0 ±0.8
Fo	0.77 ±0.00	0.78 ±0.00	0.76 ±0.01	0.89 ±0.00
Ni (ppm)	-	-	-	1573 ±426
100Mn/Fe	2.0 ±0.3	2.3 ±0.2	2.5 ±0.2	1.9 ±0.5

<sup>1</sup>n=number of analyses/sample. <sup>2</sup>WR Mg# = whole rock Mg-number. Reported uncertainties are 2σ deviations from the mean calculated from n samples.

of Alaskan-type intrusions (Taylor, 1967; Guillou-Frottier, 2014), is not well developed (Fig. 2).

#### 4.1. Serpentinized dunite

Volumetrically minor, serpentinized dunite forms light brown to beige weathering, strongly magnetic, irregularly shaped pods in wehrlite or olivine clinopyroxenite. These pods are elongate irregular bodies, metres to 10s of metres long, that locally pinch out in surrounding pyroxenite (Fig. 3a). The geometry of the pods suggests that dunite flowed plastically through the more competent wehrlite and olivine clinopyroxenite.

Dunite is completely replaced by serpentine and is, along with surrounding pyroxenite, cut by mm- to cm-wide veins of magnetite. Serpentinized dunite is predominantly composed of lizardite and veins of chrysotile ±talc, and has a density of ~2.9 g/cm<sup>3</sup>. All samples are cut by a pervasive network of magnetite microveins (Fig. 4a). Trace amounts of phlogopite, and minor, strongly-altered grains of clinopyroxene (<15% modal) occur as irregularly shaped interstitial crystals.

#### 4.2. Wehrlite

Mesocumulate wehrlite weathers brown and appears massive and black on fresh surfaces. Olivine has undergone variable degrees of serpentinization (40-90%), whereas clinopyroxene is largely fresh and unaltered.

Wehrlite is typically medium grained and contains highly fractured and irregular shaped olivine, and euhedral to subhedral clinopyroxene (0.5-0.8 cm across). Olivine grain boundaries and fractures are lined by thin coatings of secondary magnetite. Individual clinopyroxene grains commonly contain multiple inclusions of olivine, indicating early olivine crystallization (Fig. 4b). However, predominantly cotectic crystallization of the two minerals is indicated by their subequal proportions and similar crystal size, as well as the subhedral to euhedral crystal habit of clinopyroxene.

#### 4.3. Olivine ±magnetite clinopyroxenite

Brown weathering, dark green olivine clinopyroxenite is the predominant lithology of the Mount Hickman ultramafic complex (Fig. 3b). Meso- to orthocumulate olivine clinopyroxenite is medium grained, and composed chiefly of euhedral clinopyroxene (>80%), pseudomorphed olivine, and magnetite (2-10%). Well saussuritized plagioclase and biotite form local intercumulus crystals.

Clinopyroxene is generally fresh, and contains inclusions of olivine and magnetite. Cores of clinopyroxene, delineated by needles of fine magnetite, are rare. Magnetite also occurs both as irregular shaped interstitial crystals and blebby cumulus grains (Figs. 4c-d). Rare, magnetite-enriched olivine clinopyroxenite contains up to 40% interstitial, net-textured magnetite (Figs. 3c and 4e-f).

#### 4.4. Magnetite olivine gabbro

Brown weathering, mottled, medium-grained olivine gabbro was observed along the southwestern margin of the Mount Hickman ultramafic complex. The gabbro contains subequal proportions of euhedral clinopyroxene and saussuritized plagioclase (>90%), heavily altered (iddingsite) olivine (~5%), and interstitial magnetite (Fig. 4g).

A green-weathering olivine gabbro was also identified along the western margin of the exposed ultramafic. The gabbro is extensively altered, with chlorite veins (<1 mm), pervasively saussuritized plagioclase, and significant replacement of clinopyroxene by chlorite ±actinolite. Trace olivine (~1%) is completely replaced by iddingsite.

#### 4.5. Middle Scud wehrlite

The ultramafic rocks of the Middle Scud body are weakly to strongly foliated, brown to dark grey weathering, fine-grained meta-wehrlites. Metamorphism and recrystallization at the Middle Scud body vary from intensely recrystallized, fine-

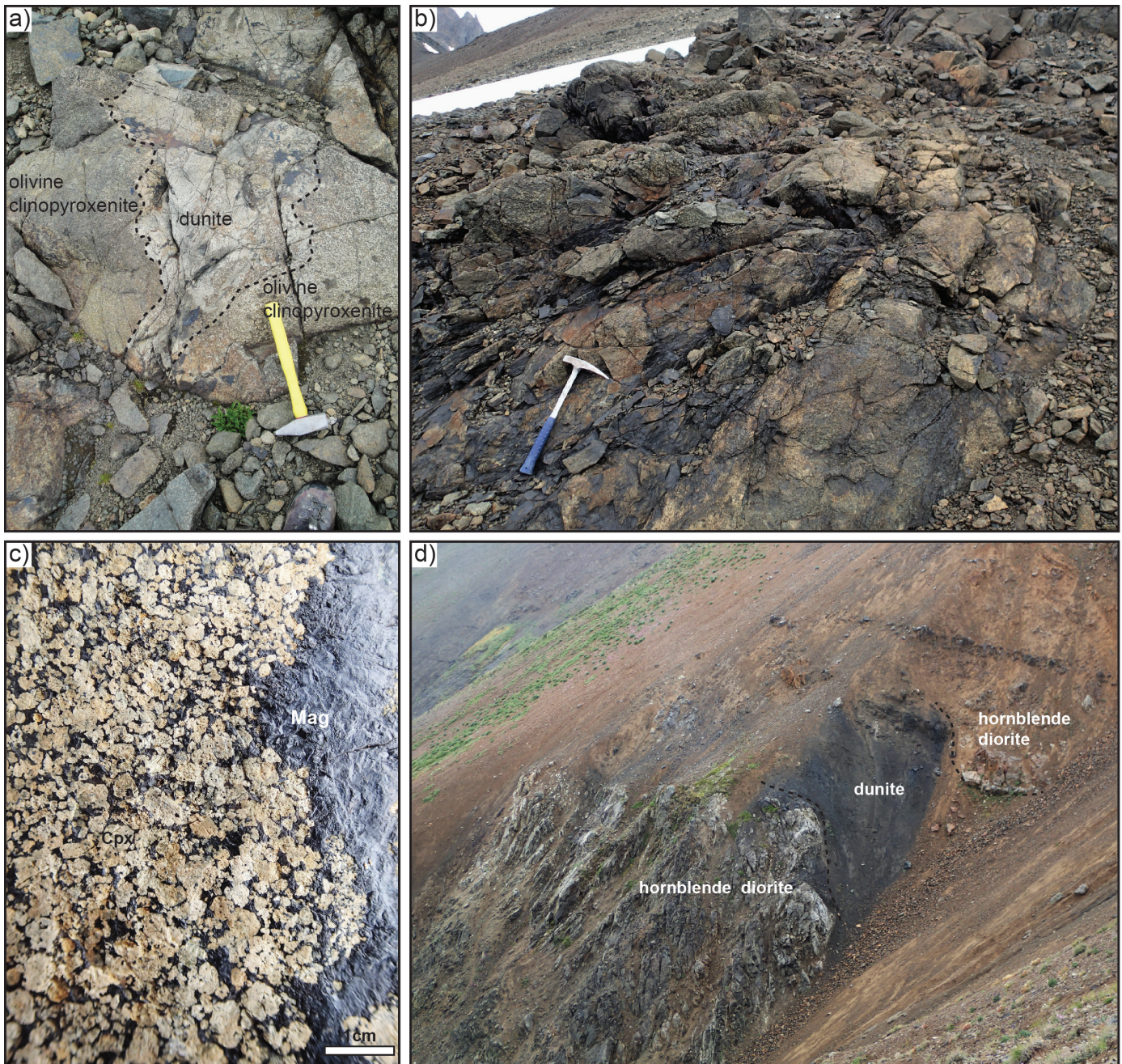


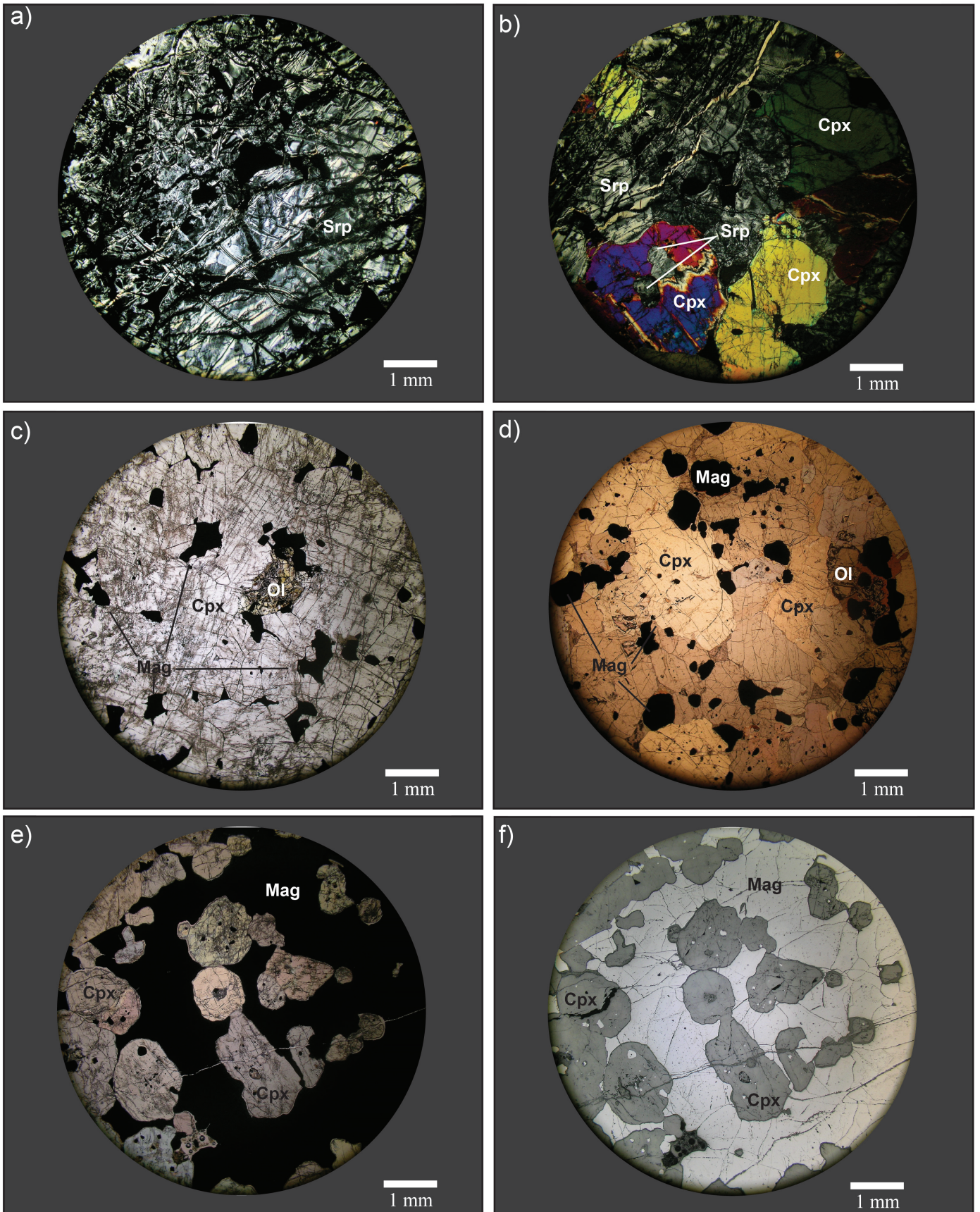
**Fig. 3.** **a)** Irregularly-shaped serpentinized dunite pod surrounded by olivine clinopyroxenite. Plates of magnetite, interpreted to be remnants of a vein are visible on the exposed serpentinized dunite surface. **b)** Brown to rust-stained rubbly outcrop of olivine clinopyroxenite. **c)** Close-up of a weathered surface of an extreme-end member of orthocumulate magnetite olivine clinopyroxenite. Cumulus crystals of beige-weathering clinopyroxene and olivine (not discernible) are hosted in intercumulus magnetite; see also Fig. 4c). A magnetite vein is visible on the right side of the photo. **d)** Black, recessive, sheared serpentinized dunite between hornblende diorite. A late basaltic dike cuts the outcrop ca. 10 m above the dunite.

grained amphibolite, composed predominantly of granoblastic polygonal amphibole and clinopyroxene, to wehrlite with well-preserved igneous cumulate textures composed predominantly of clinopyroxene and serpentinized olivine (Fig. 4h). All samples contain magnetite and variable amounts of phlogopite (up to 15%).

## 5. Geochemistry

### 5.1. Mount Hickman mafic-ultramafic complex

The rocks of the Mount Hickman ultramafic complex are crystal cumulates; consequently their geochemical composition is mainly governed by the relative proportions of constituent mafic minerals. In addition to having the highest MgO (>37 wt.%) and MgO + FeO<sup>TOT</sup> (51 wt.%) concentrations



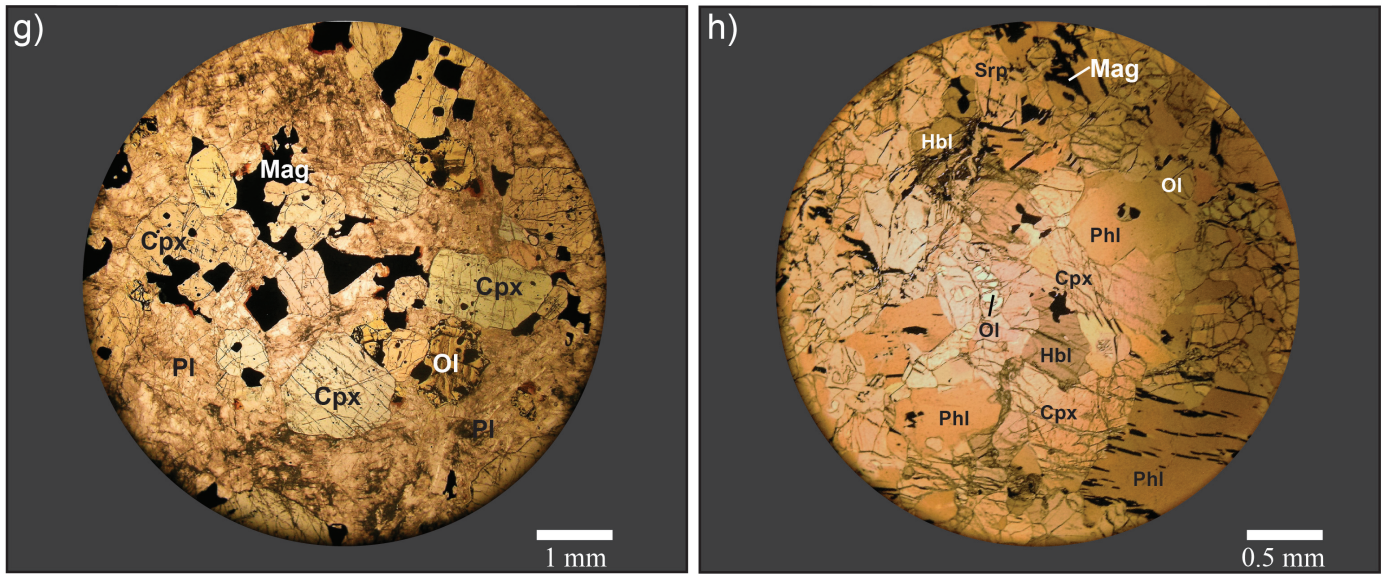


**Fig. 4.** **a)** Cross-polarized photomicrograph of a pervasively serpentinized (Srp) dunite, (sample ZE15-DM4-05A). **b)** Cross-polarized light image of wehrlite (sample ZE15-DM4-04A) consisting of mainly fresh clinopyroxene (Cpx) and serpentine. Note the euhedral inclusions of serpentinized olivine in the clinopyroxene crystal in the lower left quadrant. **c)** Plane-polarized light image of mesocumulate olivine clinopyroxenite (sample ZE15-DM4-03B), containing relatively fresh clinopyroxene, pervasively serpentinized olivine (Ol), and interstitial magnetite (Mag). **d)** Plane-polarized light image of magnetite olivine clinopyroxenite (sample ZE09-062). In contrast to the interstitial habit of magnetite grains in c), magnetite is blebby and sub-equant, suggesting cotectic crystallization with olivine and clinopyroxene. **e)** Plane-polarized light image of an orthocumulate magnetite clinopyroxenite (sample ZE15-DM04-03C). This extreme end member contains  $\leq 40\%$  magnetite. **f)** Reflected light image of e). **g)** Plane-polarized image of an olivine gabbro (sample ZE15-SB54A), comprising iddingsitized olivine, clinopyroxene, magnetite, and plagioclase (Pl). **h)** Plane-polarized light image of a phlogopite (Phl)-rich meta-wehrlite (sample ZE15-DM7-03C) from the Middle Scud ultramafic body. In addition to phlogopite, metamorphosed wehrlites from the Middle Scud body contain abundant hornblende (Hbl) after clinopyroxene, and partially serpentinized olivine.

(LOI-free), which approach those of pure olivine, dunite has the lowest abundances of  $A_2O_3$  ( $<1$  wt.%), CaO,  $Na_2O$ , and  $K_2O$  (below detection limit), and incompatible trace elements (Figs. 5 and 6) among the Mount Hickman complex rock types. Sample ZE15-DM4-08B contains ubiquitous carbonate and higher concentrations of CaO (8.5 wt.%), Sr, and LOI (16 wt.%) than other dunites (CaO  $\sim 0.10$  wt.%; LOI = 10-11 wt.%), and is thus interpreted to be significantly metasomatized. The remaining dunite samples have FeO concentrations of  $\sim 21$  wt.%, which exceed those of all other rock types, including the carbonate metasomatized dunite, and Mg-numbers (defined here as  $Mg/(Mg+Fe^{TOT})$ ) of  $\leq 0.76$ . In dunite, the concentration of Ni ranges from 450-650 ppm; Cr ranges from 850 to 2000 ppm. The concentrations of Ni in the serpentinized dunite are notable because they are significantly lower than those of most cumulate dunite samples, globally (Fig. 7a). The abundance of incompatible trace elements is low, typically between 0.1 and 1  $\times$  PM (Primitive Mantle concentrations; Palme and O'Neill, 2003), although Nb and most large ion lithophile elements (LILE) are below detection limit. Due, in part, to low absolute abundances, which approach analytical detection limits, the PM-normalized trace element profiles of the Mount Hickman complex dunite samples display significant spread and appear jagged (Fig. 6). Notably, the FeO-rich serpentinized dunites also display strong, PM-normalized, relative enrichments in  $TiO_2$  (0.2-0.3 wt.%) and may also be relatively enriched in  $P_2O_5$ ,

However, the positive P anomalies (Fig. 6) are equivocal, given the low (below quantification limit) absolute abundance of  $P_2O_5$  in the dunites. In contrast to the FeO-rich dunite samples, the carbonate-metasomatized serpentinized dunite lacks the marked relative  $TiO_2$  enrichment (Fig. 6).

Abundances of MgO (20-25 wt.%) and  $FeO^{TOT}$  (12 wt.%) in wehrlite are consistent with subequal proportions of olivine and clinopyroxene. In contrast to dunite, wehrlite samples have higher concentrations of  $Al_2O_3$  (2.0-2.5 wt.%), CaO (13-14 wt.%),  $Na_2O$ ,  $K_2O$ , and incompatible trace elements (Fig. 6), and higher Mg-numbers (0.78-0.79). They contain  $\sim 300$  ppm Ni and 1100-1400 ppm Cr. As in dunite, the abundance of Nb and LILE is typically below detection limit. Despite the low levels of Nb, the high field strength elements (HFSE) display a clear depletion trend relative to the similarly compatible rare earth elements (REE), reflecting in part, the greater incompatibility of +4 charged HFSE relative to +3 charged REE in clinopyroxene (e.g., Wood and Blundy, 2001; Francis and Minarik, 2008). Rare earth elements define a convex upward profile (Fig. 6) with middle REE (MREE) enrichments relative to heavy (HREE) and light REE (LREE). Microprobe analyses of olivine from one wehrlitic sample indicate uniform Fo content (0.78), similar to the whole-rock Mg-number, and low Ni concentrations below the detection limit of  $\sim 700$  ppm.

Samples of olivine  $\pm$  magnetite clinopyroxenite have lower abundances of MgO (11-18 wt.%) and higher abundances

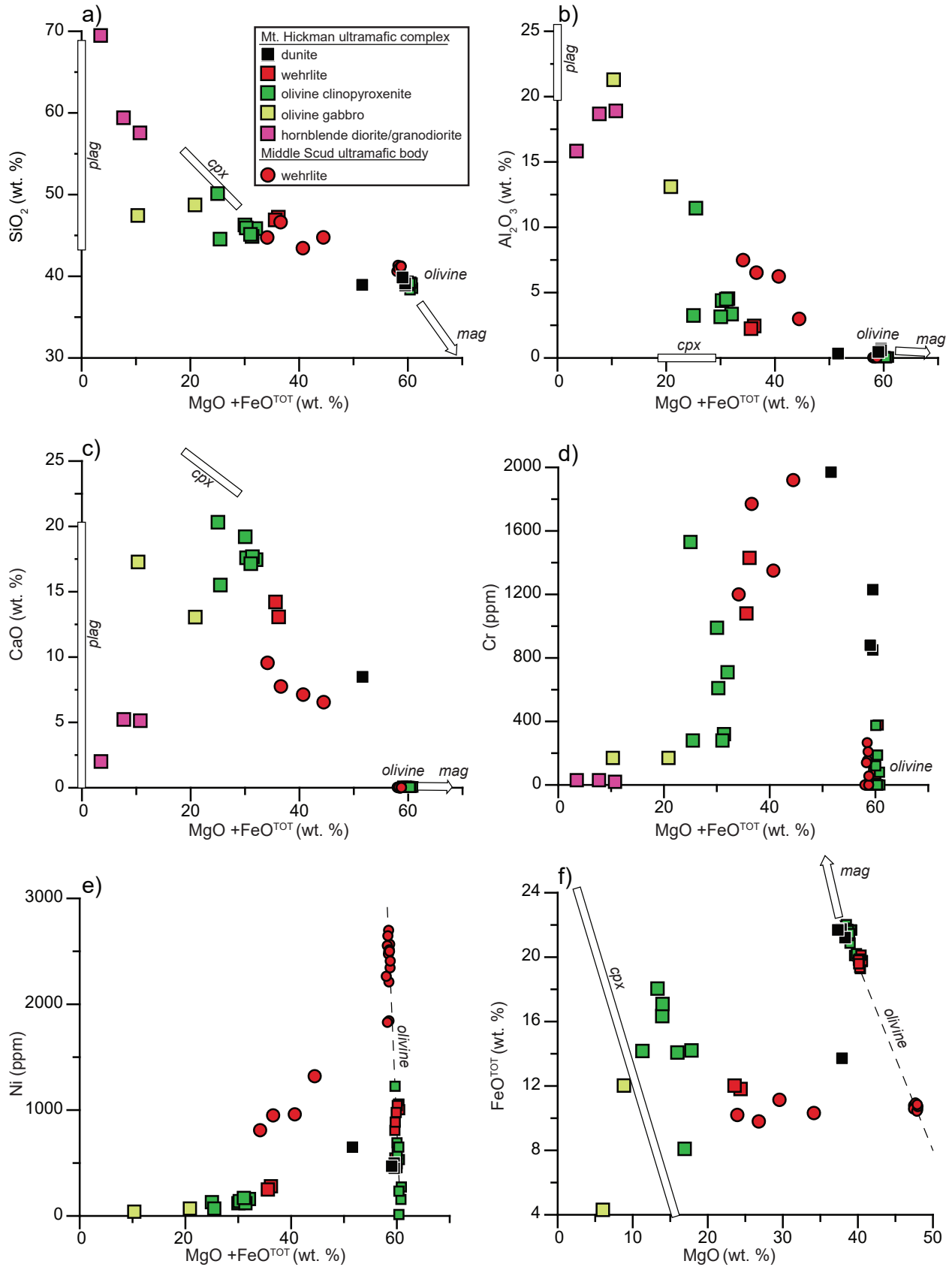


**Fig. 5.** Major and compatible trace element geochemistry of the Mount Hickman ultramafic complex and the Middle Scud ultramafic body normalized to LOI-free compositions. **a)** SiO<sub>2</sub> vs. MgO + FeO<sup>TOT</sup>. **b)** Al<sub>2</sub>O<sub>3</sub> vs. MgO + FeO<sup>TOT</sup>. **c)** CaO vs. MgO + FeO<sup>TOT</sup>. **d)** Cr vs. MgO + FeO<sup>TOT</sup>. **e)** Ni vs. MgO + FeO<sup>TOT</sup>. **f)** FeO<sup>TOT</sup> vs. MgO.

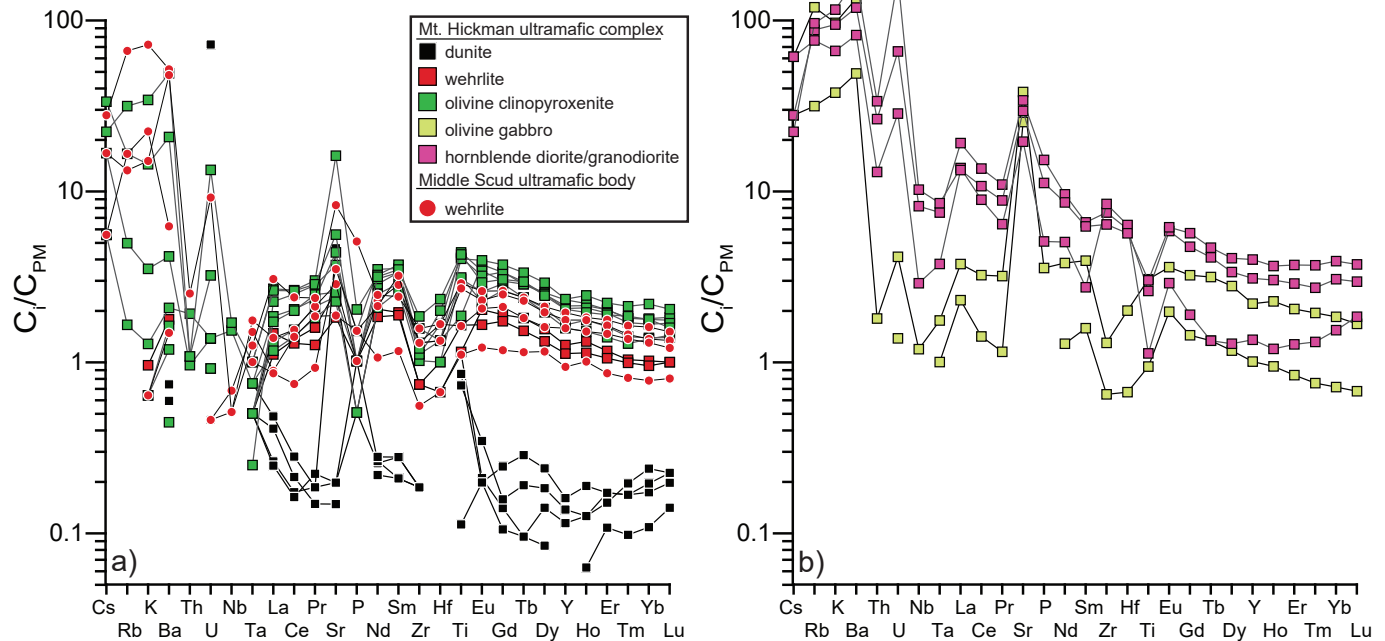


Fig. 6. Primitive mantle (Palme and O'Neill, 2003) normalized trace element profiles for **a)** ultramafic rocks of the Mount Hickman complex and Middle Scud body and **b)** gabbroic to granitic rocks of the Mount Hickman complex.

of  $\text{FeO}^{\text{TOT}}$  (8-17 wt.%),  $\text{Al}_2\text{O}_3$  (3-11 wt.%), and CaO (15.5-20.5 wt.%) than wehrlites, consistent with greater modal abundances of clinopyroxene and magnetite. Increasing FeO contents in olivine clinopyroxenite are accompanied by concomitant increases in  $\text{TiO}_2$  (0.4-1.0 wt.%), V, Sc, and Co. The incompatible trace element profiles of olivine  $\pm$ magnetite clinopyroxenites broadly resemble those of wehrlites, albeit at higher absolute concentrations. However, olivine clinopyroxenites show greater relative enrichments in MREE. Furthermore, the abundances of Ni (70-170 ppm) and Cr (300-1500 ppm) are lower than those in dunite and wehrlite. Olivine from one olivine clinopyroxenite has Fo content of 0.77 and olivine from one magnetite-rich olivine clinopyroxenite has Fo content of 0.76 Fo; both have Ni contents below detection limit.

Two samples of olivine gabbro have relatively low concentrations of MgO (6-9 wt.%) and  $\text{FeO}^{\text{TOT}}$  (4-12 wt.%), but relatively high concentrations of  $\text{Al}_2\text{O}_3$  (13-21 wt.%) and CaO (13-17 wt.%). The trace element profile of the relatively magnesian olivine gabbro is similar to those of olivine clinopyroxenite samples. However, the gabbro displays strong enrichment of Sr relative to similarly compatible trace elements. The less magnesian, relatively aluminous gabbro, shows strong relative depletion in HREE, and low absolute abundances of incompatible trace elements (except Sr), consistent with significant accumulation of plagioclase.

### 5.2. Middle Scud wehrlite

The Middle Scud ultramafic body wehrlite samples have 23-32 wt.% MgO, spanning the compositional gap between the Mount Hickman complex dunites and wehrlites. However,

the  $\text{FeO}^{\text{TOT}}$  concentrations (10-11 wt.%) of the Middle Scud wehrlites are less than those of the ultramafic rocks of the Mount Hickman complex, and require a parental magma with a higher Mg/Fe ratio, thus precluding a simple closed-system genetic relationship between the two intrusions. Three wehrlite samples (Fig. 7) have trace element profiles that overlap with those of the olivine clinopyroxenites from the Mount Hickman complex. In contrast, one sample (ZE15-DM-03F), has lower absolute incompatible trace element abundances, and displays the least relative MREE enrichment.

## 6. Discussion

The most striking characteristic of the ultramafic rocks of the Mount Hickman ultramafic complex is their relatively high  $\text{FeO}^{\text{TOT}}$  content (Fig. 8) which, at a given MgO concentration, exceeds that of most Alaskan-type intrusions in the North American Cordillera (see Findlay, 1969; Himmelberg and Loney, 1985; Scheel, 2007) and most terrestrial ultramafic rocks in general. These elevated Fe contents, however, are approached by the Duke Island Alaskan-type intrusion (Irvine, 1974) and resemble ferropicrites, a rare class of rocks whose emplacement is mainly limited to the Archean (e.g., Milidragovic and Francis, 2016). In contrast, the Middle Scud ultramafic body has relatively low whole-rock  $\text{Fe}^{\text{TOT}}$  contents and contains relatively Fo-rich olivine ( $\text{Fo}_{89}$ ), and thus resembles most Alaskan-type ultramafic intrusions. In the following we focus on dunite as the most primitive magmatic cumulate and the closest representative of the magma parental to the Mount Hickman ultramafic complex, and consider four permissible petrologic explanations for the unusually Fe-rich

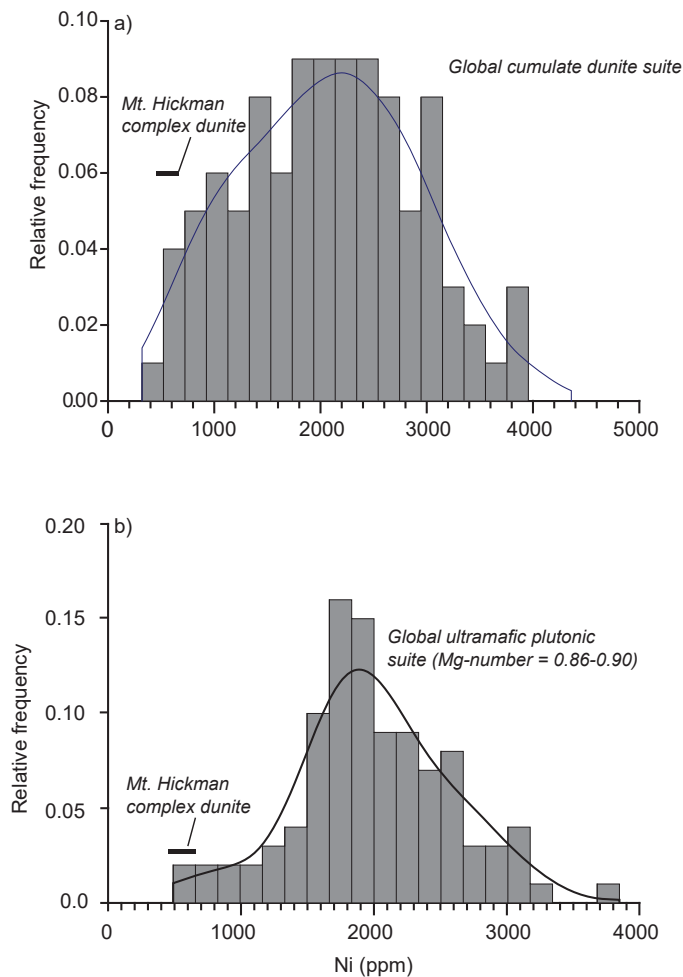


**Fig. 7.** Relative probability histogram of whole-rock Ni content from the global compilation of **a)** cumulate dunites ( $n=242$ ) and **b)** high Mg-number (0.86-0.90) cumulates ( $n=170$ ; MgO >27 wt.%). Source: GEOROC database (<http://georoc.mpch-mainz.gwdg.de>), accessed on Nov. 15<sup>th</sup>, 2016.

character of the complex: 1) alteration and element mobility; 2) evolution of a primary magma towards Fe-enrichment; 3) remobilization of cumulates from original Fe-rich olivine layers; and 4) magma mixing.

### 6.1. Alteration and element mobility

The ultramafic rocks of the Mount Hickman ultramafic complex have been extensively serpentinized and contain widespread veins of magnetite raising the possibility of significant element mobility, including Fe and Ni. Therefore, one possible explanation for the high content of FeO<sup>TOT</sup> in dunites from the Mount Hickman ultramafic complex is metasomatic enrichment by Fe-rich melts and fluids. The relative enrichment of Ti  $\pm$  P in dunites (Fig. 6), further suggests metasomatism by Fe-Ti-P-rich fluids or immiscible melts, similar to those attributed to late-stage magmatic liquid immiscibility in slowly cooled mafic intrusions elsewhere (Philpotts, 1982; Jakobsen et al., 2005; Zhou et al., 2013). Similarly, mobility of Ni to form secondary Ni-sulphide (millerite, heazlewoodite), Ni-arsenide

(nickeline) or Ni-Fe alloy (awaruite) may account for the low absolute concentrations of Ni (<650 ppm) in serpentinized dunites of the Mount Hickman ultramafic complex. However, mass balance calculations indicate that metasomatism alone may not account for FeO-rich rocks in the complex.

Mass balance calculations, based on the assumption that serpentinization of Mount Hickman dunites did not directly result in MgO-loss or FeO-gain, indicate that the observed high FeO<sup>TOT</sup> concentrations of the Mount Hickman complex dunite would require the addition of 6-10 mol.% FeO as magnetite to 'normal' dunite with Mg-number of 0.86-0.90 (Fig. 8). Assuming average serpentine and magnetite density of 2.55 g/cm<sup>3</sup> and 5.2 g/cm<sup>3</sup>, respectively (Deer et al., 1969), such metasomatically Fe-enriched dunites would comprise ~10-20 vol.% magnetite; modal magnetite abundance in samples collected for geochemical analysis is significantly lower than this. Furthermore, the density of analyzed dunite samples (~2.9 g/cm<sup>3</sup>) suggests that the maximum magnetite content (assuming pure Mg-serpentine) and no clinopyroxene and/or chromite is ~10%.

Based on these considerations, the origin of the FeO-rich dunite of the Mount Hickman ultramafic complex solely through post-crystallization metasomatic enrichment of 'normal' dunite (Mg-number=0.86-0.90) appears unlikely. Instead, metasomatic addition of FeO, if significant, operated on a dunitic precursor with a relatively low Mg-number ( $\leq 0.86$ ; Fig. 8). Regardless of the exact amount of metasomatic FeO addition, the FeO-rich nature of the Mount Hickman ultramafic rocks must, in part, reflect the original FeO-rich character of their parental magmas.

### 6.2. Evolution of primary magma towards Fe-enrichment

The Fe-rich, Ni-poor character of the Mount Hickman complex dunite may reflect an earlier history of magmatic differentiation and olivine fractionation. Although fractionation of sulphide  $\pm$  Cr-spinel results in efficient Ni removal from melts, extensive fractionation of either phase is inconsistent with the Fe-rich character of dunite. The exact amount of fractionation necessary for the observed Fe-enrichment is impossible to determine. However, some robust inferences using olivine-liquid Fe-Mg equilibria (cf. Roeder and Emslie, 1970) and the minimum MgO-content of the parental liquid saturated in olivine only (~10 wt.% MgO), may be drawn. An olivine-saturated magma, parental to the Fe-rich dunite of the Mount Hickman mafic-ultramafic complex, requires an Mg/(Mg+Fe<sup>2+</sup>) ratio of 0.49, and a corresponding minimum FeO<sup>TOT</sup> concentration of 19 wt.% to produce adcumulate dunite with a whole-rock Mg-number of ~0.76. Such Fe-rich magmas are restricted to Archean ferropicrites and cannot be produced by olivine fractionation from primary liquids generated by melting of normal pyrolitic mantle (Milidragovic and Francis, 2016). Consequently, it is unlikely that dunites of the Mount Hickman ultramafic complex formed by accumulation of olivine from an evolved residual magma derived from high Mg-number (>0.65) primary melts by closed system fractional crystallization.

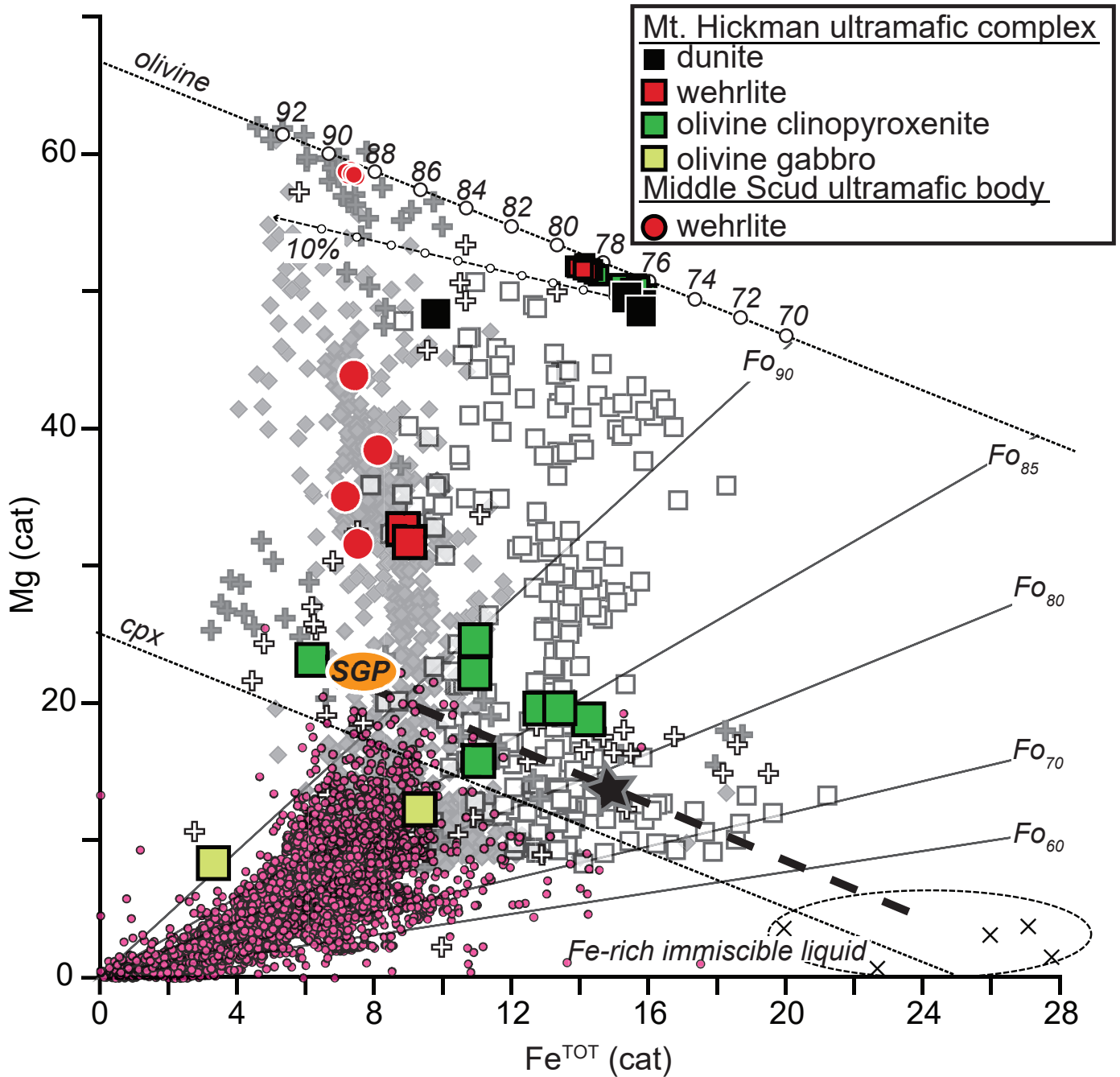


**Fig. 8.** Mg vs.  $Fe^{TOT}$  in cation units, showing the compositions of rocks (large symbols) and olivine (small symbols) from the Mount Hickman complex and the Middle Scud body. Electron microprobe-determined olivine compositions are shown by the smaller symbols along the olivine stoichiometric line (negatively sloping dashed line near the top of diagram). Also shown is the clinopyroxene stoichiometric line (cpx), and the isopleths of constant Fo content coexisting with liquids as determined by the Fe-Mg exchange coefficient ( $K_D=0.30$ ) and adjusted for  $Fe^{2+}/Fe^{TOT}=0.15$ . The effect of post accumulation magnetite metasomatism (0-10%) is illustrated by the dashed line emanating from the Mount Hickman complex dunite. Other data: pink circles – calcalkaline volcanic suite from Andes arc ( $n=5339$ ; <http://georoc.mpch-mainz.gwdg.de>); grey diamonds – mafic and ultramafic rocks with pyroclitic (Mg-number=0.88-0.92) mantle provenance (Milidragovic and Francis, 2016); white squares – Archean ferropicrites from the Superior Province (Milidragovic and Francis, 2016); grey crosses – Alaskan-type intrusions (Findlay, 1969; Himmelberg and Loney, 1995; Scheel, 2007); white crosses – Fe-rich Alaskan-type intrusions (Irvine, 1974; Himmelberg and Loney, 1995); x – average Fe-rich immiscible liquids compiled by Jakobsen et al. (2005); SGP=parental composition of the Stuhini Group picrite determined by Milidragovic et al. (2016b). Black star – hypothetical magma in equilibrium with  $Fo_{76}$  and parental to the Mount Hickman complex dunites, formed by mixing between an olivine-saturated basalt and an Fe-rich immiscible liquid (thick dashed line).

### 6.3. Remobilization of transient Fe-rich dunite layers

The decimetre to metre-scale serpentized dunite units observed in the complex (see above) could conceivably represent remobilized olivine-rich layers within wehrlite or olivine clinopyroxenite, thus explaining the lack of a well-developed dunite core. Macro-scale layering is a signature of large layered intrusions (e.g., Muskox Intrusion; Irvine and Smith, 1967); remobilization of olivine-rich cumulate layers has been inferred at the Turnagain and Tulameen complexes (Nixon et al., 1997; Scheel, 2007; Nixon et al., 2012). Layers of dunite with relatively low Mg-number may be generated by mixing of relatively evolved, clinopyroxene-saturated liquids with primitive, olivine-saturated, magmas (e.g., Irvine, 1979), and thus represent transient deviations from the olivine-clinopyroxene cotectic. Mixing between differentiated and primitive liquids may also explain the low concentrations of Ni in dunite without invoking Ni mobility and secondary Ni mineralization.

We consider that such remobilization is unlikely because the high Fe content of Mount Hickman complex dunites appears to require a parental magma with low Mg-number and  $\text{FeO}^{\text{TOT}} \geq 19$  wt.%, and the calc-alkaline magma (indicated by the observed crystallization sequence of olivine, clinopyroxene, magnetite, plagioclase) would have been unable to reach the implied level of Fe-enrichment (Fig. 8). Furthermore, mixing between primitive and evolved magmas fails to readily explain the relative enrichment of  $\text{TiO}_2$  in serpentized dunites, because neither the primitive or differentiated liquids would be enriched in Ti relative to the similarly incompatible elements. The problem would be further compounded if the differentiated liquids were co-saturated in magnetite, whose fractionation would result in relative  $\text{TiO}_2$  depletion.

### 6.4. Magma mixing

We favour a model in which the Mount Hickman mafic-ultramafic complex was generated by two fundamentally different and unrelated, magma types. The abundant, fresh to pervasively altered, olivine and clinopyroxene cumulus crystals indicate crystallization from a silicate, mafic to ultramafic, parental liquid. However, the rounded and embayed clinopyroxene crystals in intercumulus magnetite (Figs. 4e-f), suggest that clinopyroxene was not in equilibrium with the Fe-oxide -saturated magma that occupied the interstitial space. Based on these observations, we infer the coexistence of a relatively evolved (Ni-poor), olivine  $\pm$ clinopyroxene-saturated picritic to basaltic silicate magma and magma with high normative magnetite content. Accordingly, we attribute the Fe-rich character of the ultramafic rocks to mixing of these two fundamentally different magmas at different stages of the complex's evolution. The Fe-rich oxide magma, was also likely enriched in Ti  $\pm$ P, accounting for the marked relative enrichments of these elements in the otherwise refractory dunite.

Fe-Ti-P rich glassy globules and melt inclusions, resulting from immiscible separation of Fe- and Si-rich melts from

relatively evolved tholeiitic and alkaline magmas have been observed from a range of volcanic suites (Philpotts, 1982) and mafic intrusions (Jakobsen et al., 2005; Zhou et al., 2013). Based on work in Skaergaard intrusion, Jakobsen et al. (2005) proposed mixing of dense Fe-rich liquids with primitive basaltic magmas to explain the origin of ferropicrites. However, immiscible separation of Fe-rich liquids, requires relatively reducing conditions, which inhibit early magnetite crystallization (Philpotts, 1982). Furthermore, magmatic evolution towards Fe-rich liquid immiscibility is unlikely to be achieved through a calc-alkaline (olivine-clinopyroxene-plagioclase) crystallization sequence, which is exhibited by the Mount Hickman ultramafic complex, and is instead more consistent with tholeiitic (olivine-plagioclase-clinopyroxene) differentiation.

The mixing process proposed herein requires the separation of a dense, immiscible Fe-rich liquid from a relatively evolved, dry, and reduced magma at low pressure, where plagioclase, rather than clinopyroxene, is stable (see Grove and Baker, 1984). However, the calc-alkaline crystallization sequence exhibited by the Mount Hickman complex, indicates a relatively hydrous and oxidizing ultramafic magma (see Sisson and Grove, 1993). Thus we propose that the immiscible Fe-rich liquid sank into the crust, as proposed by Jakobsen et al. (2005) for the genesis of ferropicrites, and mixed with liquid to partially crystalline picritic to basaltic magma to form an Fe-rich, olivine-saturated hybrid magma that was parental to the dunites of the Mt. Hickman ultramafic complex.

## 7. Conclusions

The Mount Hickman ultramafic complex is a composite, Middle to Late Triassic, Alaskan-type intrusion comprising dunite, wehrlite, olivine clinopyroxenite and gabbro. With pervasively serpentized dunite and nearly fresh olivine  $\pm$ magnetite clinopyroxenite, the intrusion is variably altered. The ultramafic rocks have  $\text{FeO}^{\text{TOT}}$  contents that exceed most terrestrial ultramafic rocks, including other Alaskan-type intrusions from the North American Cordillera. The high whole-rock  $\text{FeO}^{\text{TOT}}$  concentrations are in stark contrast to the nearby (~15 km) Middle Scud ultramafic body. Of the four possibilities considered (metasomatism, magmatic differentiation, remobilization of cumulates from original Fe-rich olivine layers, and magma mixing), field, petrographic, and geochemical evidence leads us to favour a preliminary model in which the unusual Fe-enrichment of the Mount Hickman ultramafic complex resulted from mixing of two magma types: a relatively evolved picritic/basaltic magma and a Fe-Ti-P-rich liquid similar to the glassy globules and melt inclusions reported from elsewhere by Philpotts (1982) and Jakobsen et al. (2005). The proposed model may be tested by in-situ analysis of melt inclusions hosted in clinopyroxene crystals from the Mount Hickman ultramafic complex and identification of a population with strong Fe enrichment, similar to that reported by Jakobsen et al. (2005) and references therein (Fig. 8). An expanded global geochemical database of Alaskan-type intrusions combined

with further study of magnetite, clinopyroxene, and trapped melt inclusions from the Mount Hickman Complex will help address the origin of ultramafic intrusions at convergent margins and aid understanding, and exploring for, magmatic Ni-Cu-PGE mineralization of Alaskan-type intrusions.

### Acknowledgments

This study was funded by the Government of Canada's Geomapping for Energy and Minerals program (ESS contribution number 20160198). Logistical support was generously provided by Teck Resources, and we with particularly thank Klaus Heppel, Gabe Jutras, and Leif Bailey. The authors benefited from excellent field assistance by Simon Carroll and Sebastian Bichlmaier. We thank Graham Nixon for perceptive comments to a first draft and, in particular, for pointing out misconceptions tied to the term 'Polaris suite' and for challenging us with possible alternative origins.

### References cited

- Barresi, T., Nelson, J.L., Dostal, J., and Friedman, R., 2015. Evolution of the Hazelton arc near Terrace, British Columbia: stratigraphic, geochronological, and geochemical constraints on a Late Triassic-Early Jurassic arc and Cu-Au belt. *Canadian Journal of Earth Sciences*, 52, 466-494.
- Brown, D.A. and Gunning, M.H., 1989. Geology of the Scud River area, northwestern British Columbia (104G/5 and 6). In: *Geological Fieldwork 1988*, British Columbia Ministry of Energy, Mines and Petroleum Resources, British Columbia Geological Survey Paper 1989-1, pp. 251-267.
- Brown, D.A., Gunning, M.H., and Greig, C.J., 1996. The Stikine project: geology of the western Telegraph Creek map area, Northwestern British Columbia (NTS 104G/5, 6, 11W, 12 and 13). *British Columbia Ministry of Energy, Mines and Natural Gas, British Columbia Geological Survey Bulletin 95*, 175 p.
- Deer, W.A., Howie, R.A., Zussman, J., 1969. *An introduction to the rock forming minerals*, 4<sup>th</sup> Edition, John Wiley and Sons Inc., New York, 528 p.
- Findlay, D.C., 1969. Origin of the Tulameen ultramafic-gabbro complex, southern British Columbia. *Canadian Journal of Earth Sciences*, 6, 399-425.
- Francis, D. and Minarik, W., 2008. Aluminum-dependent trace element partitioning in clinopyroxene. *Contributions to Mineralogy and Petrology*, 156, 439-451.
- Grove, T. and Baker, M.B., 1984. Phase equilibrium controls on the tholeiitic versus calc-alkaline differentiation trends. *Journal of Geophysical Research*, 89, 3253-3274.
- Guillou-Frottier, L., Burov, E., Augé, T., Gloaguen, E., 2014. Rheological conditions for emplacement of Ural-Alaskan-type ultramafic complexes. *Tectonophysics*, 631, 130-145.
- Himmelberg, G.R. and Loney, R.A., 1995. Characteristics and petrogenesis of Alaskan-type ultramafic- mafic intrusions, southeastern Alaska. *U.S. Geological Survey Professional Paper 1564*, 51 p.
- Hirth, G. and Guillot, S., 2013. Rheology and tectonic significance of serpentinite. *Elements*, 9, 107-113. In: *Geological Fieldwork 1988*, British Columbia Ministry of Energy, Mines and Petroleum Resources, British Columbia Geological Survey Paper 1989-1, pp. 429-442.
- Holbek, P.M., 1988. *Geology and mineralization of the Stikine Assemblage, Mess Creek Area, northwestern British Columbia*. Unpublished M.Sc. thesis, The University of British Columbia, 184 p.
- Irvine, T.N., 1974. Petrology of the Duke Island ultramafic complex, southeastern Alaska. *The Geological Society of America Memoir* 138, 240 p.
- Irvine, T.N., 1979. Rocks whose composition is determined by crystal accumulation and sorting. In: H.S.Jr., Yoder (Ed.), *The Evolution of Igneous Rocks: Fiftieth Anniversary Perspectives*. Princeton University Press, Princeton, pp. 245-306.
- Irvine, T.N. and Smith, C.H., 1967. The ultramafic rocks of the Muskox intrusion, Northwest Territories, Canada. In: P.J. Wyllie (Ed.), *Ultramafic and Related Rocks*. John Wiley and Sons Inc., New York, pp. 38-49.
- Jakobsen, J.K., Veksler, I.V., Tegner, C., and Brooks, C.K., 2005. Immiscible iron- and silica-rich melts in basalt petrogenesis documented in Skaergaard intrusion. *Geology*, 33, 885-888.
- Mihalynuk, M.G., Bellefontaine, K.A., Brown, D.A., Logan, J.M., Nelson, J.L., Legun, A.S. and Diakow, L.J., 1996. *Geological compilation, northwest British Columbia (NTS 94E, L, M; 104F, G, H, I, J, K, L, M, N, O, P; 114J, O, P)*. BC Ministry of Energy and Mines, British Columbia Geological Survey Open File 1996-11.
- Milidragovic, D. and Francis, D., 2016. Ca. 2.7 Ga ferropicritic magmatism: A record of Fe-rich heterogeneities during Neoproterozoic global mantle melting. *Geochimica et Cosmochimica Acta*, 185, 44-63.
- Milidragovic, D., Joyce, N.L., Zagorevski, A., and Chapman, J.B., 2016a. Petrology of explosive Middle-Upper Triassic ultramafic rocks in the Mess Creek area, northern Stikine terrane. In: *Geological Fieldwork 2015*, British Columbia Ministry of Energy and Mines, British Columbia Geological Survey Paper 2016-1, pp. 95-111.
- Milidragovic, D., Chapman, J.B., Bichlmaier, S., Canil, D., and Zagorevski, A., 2016b. H<sub>2</sub>O-driven generation of picritic melts in the Middle to Late Triassic Stuhini arc of the Stikine terrane, British Columbia, Canada. *Earth and Planetary Science Letters* 454, 65-77.
- Nixon, G.T., Ash, C.H., Connely, J.N., and Case, G., 1989. Alaskan-type mafic-ultramafic rocks in British Columbia: the Gnat Lakes, Hickman, and Menard Creek complexes. In: *Geological Fieldwork 1988*, British Columbia Ministry of Energy, Mines and Petroleum Resources, British Columbia Geological Survey Paper 1989-1, pp. 429-442.
- Nixon, G.T., Hammack, J.L., Ash, C.H., Cabri, L.J., Case, G., Connely, J.N., Heaman, L.M., Laflamme, J.G.H., Nuttall, C., Paterson, W.P.E., and Wong, R.H., 1997. Geology and platinum-group-element mineralization of Alaskan-type ultramafic- mafic complexes in British Columbia. *British Columbia Ministry of Employment and Investment, British Columbia Geological Survey Bulletin 93*, 141 p.
- Nixon, G.T., Hitchens, A.C., Ross, G.P., 2012. Geology of the Turnagain ultramafic intrusion, Northern British Columbia; BC Ministry of Energy and Mines, Open File 2012-05, map 1:10,000 scale.
- Nixon, G.T., Manor, M.J., Jackson-Brown, S., Scoates, J.S., and Ames, D.E., 2015. Magmatic Ni-Cu-PGE sulphide deposits at convergent margins, In: D.E. Ames and M.G. Houlé (Eds.), *Targeted Geoscience Initiative 4: Canadian Nickel-Copper-Platinum Group Elements-Chromium Ore Systems — Fertility, Pathfinders, New and Revised Models*. Geological Survey of Canada, Open File 7856, pp. 17-34.
- Palme, H. and O'Neill, H.St.C., 2003. Cosmochemical estimates of mantle composition. In: Holland, H.D., Turekian, K.K., Davis, A.M. (Eds.), *Treatise on Geochemistry*, vol. 2. Elsevier, Amsterdam, The Netherlands, pp. 1-38.
- Philpotts, A.R., 1982. Compositions of immiscible liquids in volcanic rocks. *Contributions to Mineralogy and Petrology*, 80, 201-218.
- Roeder, P.L. and Emslie, R.F., 1970. Olivine-liquid equilibrium. *Contributions to Mineralogy and Petrology*, 29, 275-289.
- Scheel, J.E., 2007. Age and origin of the Turnagain Alaskan-type

- intrusion and associated Ni-sulphide mineralization, north-central British Columbia, Canada. Unpublished M.Sc. thesis, The University of British Columbia, 211 p.
- Sisson, T.W. and Grove, T.L., 1993. Experimental investigations of the role of H<sub>2</sub>O in calc-alkaline differentiation and subduction zone magmatism. *Contributions to Mineralogy and Petrology*, 113, 143-166.
- Taylor, H.P.Jr., 1967. The zoned ultramafic complexes of southeastern Alaska. In: P.J. Wyllie (Ed.), *Ultramafic and Related Rocks*. John Wiley and Sons Inc., New York, p. 97-121.
- Wood, B.J. and Blundy, J.D., 2001. The effect of cation charge on crystal-melt partitioning of trace elements. *Earth and Planetary Science Letters*, 188, 59-71.
- Woodsworth, G. J., Anderson, R. G., and Armstrong, R. L., 1991. Plutonic regimes, in Gabrielse, H., and Yorath, C. J., (Eds.), *Geology of the Cordilleran Orogen in Canada, Volume Geology of Canada 4*, Geological Survey of Canada, p. 491-531.
- Zagorevski, A., Mihalynuk, M.G., Milidragovic, D., Joyce, N., Kovacs, N., Allan, M., and Kellett, D., 2016. Characterization of volcanic and intrusive rocks across the British Columbia - Yukon border, GEM2 Cordillera. Geological Survey of Canada, Open File 8141, 13 p. doi:10.4095/299198.
- Zhou, M.-F., Chen, W.T., Wang, C.Y., Prevec, S.A., Liu, P.P., and Howarth, G.H., 2013. Two stages of immiscible liquid separation in the formation of Panzhihua-type Fe-Ti-V oxide deposits, SW China. *Geoscience Frontiers* 4, 481-502.